Half-Pulse Excitation Pulse Design and the Artifact Evaluation

Phillip Cho

1. INTRODUCTION

A conventional excitation scheme consists of a slice-selective RF excitation followed by a gradient-refocusing interval (zero order moment nulling; negative lobe). However, this excitation is often limited by the finite duration of the selective excitation, the large gradients required for thin-slice excitation, and the subsequent refocusing and flow-compensation gradients. These limitations restrict the minimum achievable TE and cause displacement artifacts and flow-dependent phase shifts, resulting in artifactual signal loss, distortion, and poorer flow depiction [1–3].

These problems can be resolved by using a half-pulse excitation scheme proposed by Pauly et al.[4]. This method provides significant reductions in spin dephasing, and eliminates moment nulling following the excitation, so it reduces the amount of gradient action prior to readout and permits ultra-short echo times on the order of 250~300 μsec.

2. THEORY

2.1 CONVENTIONAL PULSE EXCITATION & SEQUENCE

A conventional excitation scheme is illustrated in Figure 1. The excitation imposes a weighting in excitation k-space along a linear trajectory defined between k-space points k_{min} and k_{max}. Refocusing subsequently centers the weighting function about the origin in k-space. As shown in Figure 1(c), the amplitude of the applied RF pulse decays with rate $T2^*$ during gradient-refocusing interval. This Effect of $T2^*$ in RF pulse causes the loss of signal and the loss of selectivity. To minimize $T2^*$ decay, we should minimize echo time (TE).

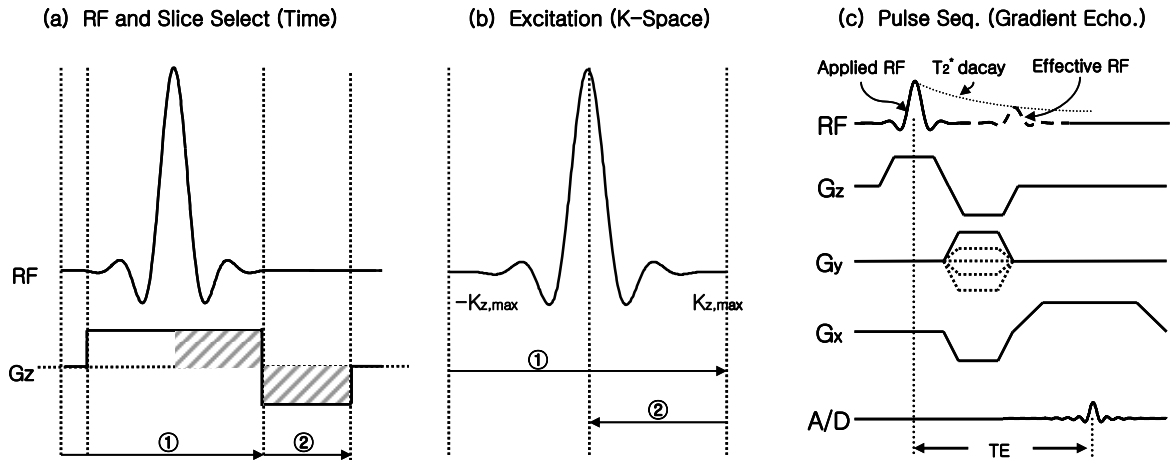

Figure 1 Conventional excitation scheme

2.2 HALF-PULSE EXCITATION & SEQUENCE

The half-pulse selective excitation scheme is illustrated in Figure 2 and consists of two excitations, each scanning half of excitation k-space. The first half-excitation, played out in the presence of a positive gradient, begins at the k-space minimum k_{min} and ends at the k-space origin while imposing a k-space weighting equivalent to a centrically truncated conventional RF pulse.

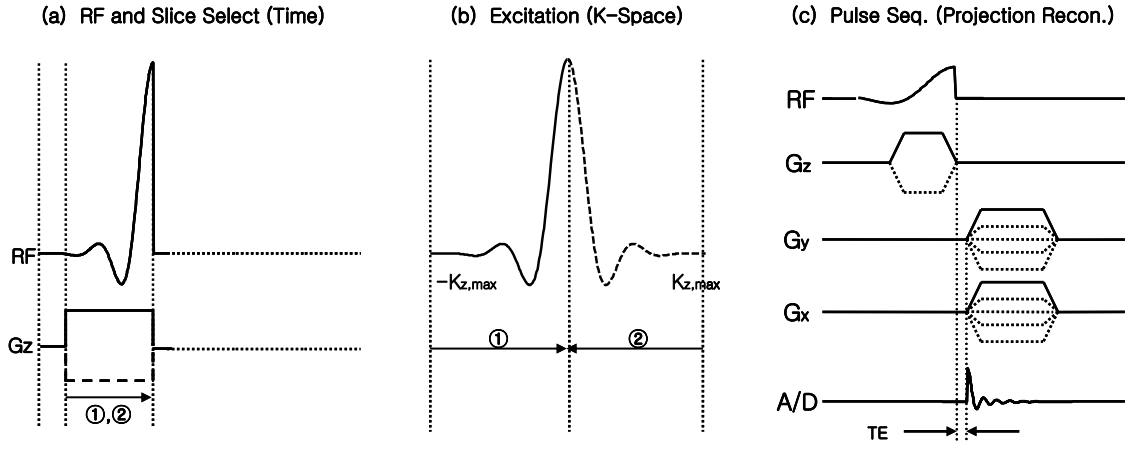

Figure 2 Half-pulse excitation scheme

Data acquisition occurs after each half-excitation. The same readout gradients are applied for each pair of half-excitations, and the two individual measurements are summed. In the absence of irregularities (such as field inhomogeneities or eddy currents), the resultant signal is the same as that generated by the corresponding conventional excitation.

Compared to previous Figure 1(c) from conventional excitation, we can see TE is very small in Figure 2(c). Because each half-excitation concludes at the ‘‘peak’’ of the excitation, at which the bulk of the transverse magnetization has been created, the gradient moment at the end of the excitation is zero. As a result, the need for moment nulling is eliminated and no refocusing or first-order flow compensation is required. The shorter TE significantly reduces spatial displacement artifacts.

The half-pulse excitation technique may be combined with any acquisition trajectory. However, combining the half-pulse excitation with a half-echo radial-line acquisition (e.g., projection reconstruction, twisting radial lines (TwiRL), spirals) maximizes the benefits of the resultant sequence with respect to flow imaging [5].

2.3 PROFILE SYNTHESIS OF HALF PULSES.

The Fourier interpretation of the excitation k-space formalism is also useful to illustrate the behavior of the half-pulse excitation. According to this interpretation, the excitation response, or slice profile, of a conventional pulse $b(t)$ is determined by the Fourier transform of $b(t)$, denoted $B(s)$:

The slice profile $M_{xy}(z)$ is simply proportional to the Fourier transform of the weighted k-space trajectory,

$$M_{xy}(z) \propto B(s)$$

In the same manner, the excitation response of ‘‘half’’ of the RF pulse is determined by taking the Fourier transform of $b^{+}(t)=b(t)u(t)$, where $u(t)$ is the unit step function defined as 1 for t>0 and 0 for t<0. The predicted slice profile $B^{+}(s)$ of the half-pulse excitation is, therefore

$$b^{+}(t) \Leftrightarrow B^{+}(s) = B(s) * U(s) = B(s) * \left[\frac{1}{2}\delta(s) - i\frac{1}{2\pi s} \right] = \frac{1}{2}\left[B(s) + iB_{Hi}(s) \right]$$

where $B_{Hi}(s)=B(s)*(-1/\pi s)$ is the Hilbert transform of $B(s)$, and * denotes convolution. Similarly, the ‘‘second half’’ of the RF pulse, defined as $b^{-}(t)=b(t)u(-t)$ has a slice profile $B^{-}(s)$,

$$b^{-}(t) \Leftrightarrow B^{-}(s) = B(s) * U(-s) = B(s) * \left[\frac{1}{2}\delta(s) + i\frac{1}{2\pi s} \right] = \frac{1}{2}\left[B(s) - iB_{Hi}(s) \right]$$

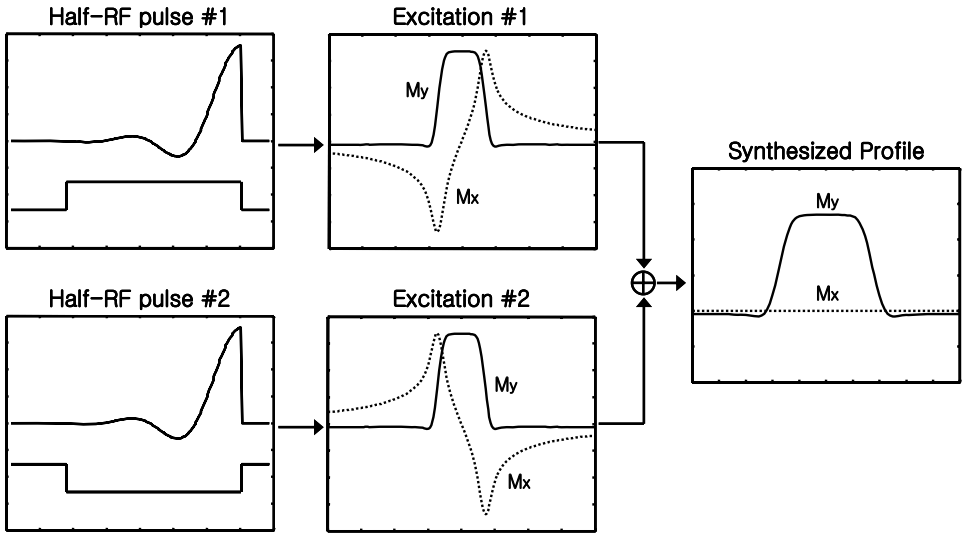

Figure 3 Synthesized profile after two half-pulse excitations

As the equations indicate, truncation of the conventional excitation at its center results in the addition of an undesired term, which is the Hilbert transform of the desired response. For a real, symmetric RF pulse shape $b_e(t)$, of which the Fourier transform is also real and symmetric, the undesired term is imaginary and asymmetric. However, the two half-excitations are pieced together, that is, the sum $b^+(t) + b^-(t) = b(t)$ results in an excitation k-space weighting equivalent to the full-pulse weighting. Since the Fourier transform is a linear operation, it follows that $B^+(s) + B^-(s) = B(s)$; therefore, as Figure 3 illustrates, the desired symmetric slice profile M_y is synthesized by the summation of the two component profiles, which have asymmetric parts M_x that cancel. The summation-synthesis result also holds for large tip-angle real-valued pulses. In general, the result is true for any real-valued excitation pulse, regardless of the tip angle or the time symmetry of the pulse. In this case, the spatial response of real-valued $b(t)$ is skew-Hermitian symmetric:

$$M_x(-z) = -M_x(z) \quad , M_y(-z) = M_y(z) \quad , M_z(-z) = M_z(z)$$

If off-resonance effects are ignored, the resultant magnetization arising from the sum of the responses of an excitation and its gradient-negated complement is $[0 \quad 2M_y(z) \quad 2M_z(z)]$. Again, we note that the synthesis of the desired profile M_y is accomplished while the undesired M_x components cancel and are not observed.

3. BLOCH EQUATION SIMULATION RESULTS

3.1 RF PULSES & SLICE PROFILES

The left side of Figure 4 represents applied, effective and half RF pulses and the right side of same figure represents slice profiles of each pulse for on-resonance. The slice select gradient is set to 1G/cm.

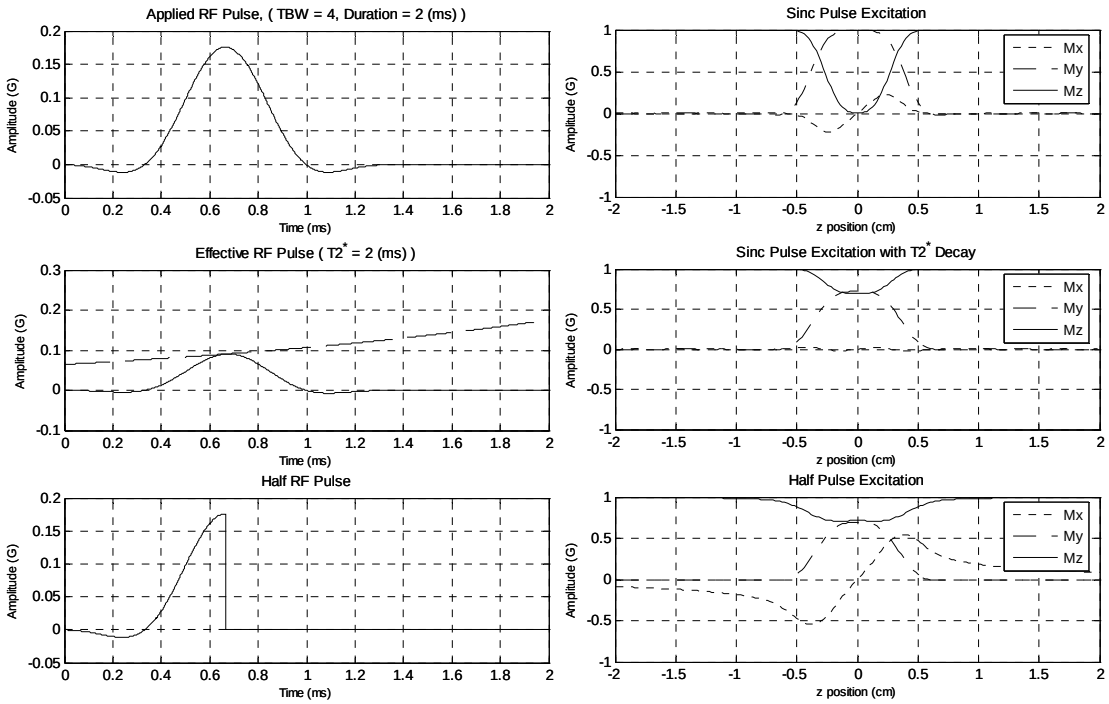

Figure 4 RF pulses & Slice Profiles (TBW=4, Duration=2ms)

The applied RF pulse is a hamming windowed sinc π/2 pulse of TBW=4 and 2ms. The effective RF pulse is a same applied RF but with $T2^*$ decay. We can see that the amplitude of effective RF smaller than applied RF and M_y component of the magnetization also has less than 1. The half RF pulse is a truncated version of the applied RF pulse and its slice profile is well refocused without negative gradient as expected.

Like Figure4, Figure5 shows RF pulses & slice profiles in the case of TBW is 8 and duration is 4ms. Because we increase both duration and bandwidth of these pulses, more selective profiles can be seen in Figure 5. We can see the M_y component of the magnetization in this effective RF pulse here much less than the previous effective RF one due to longer duration.

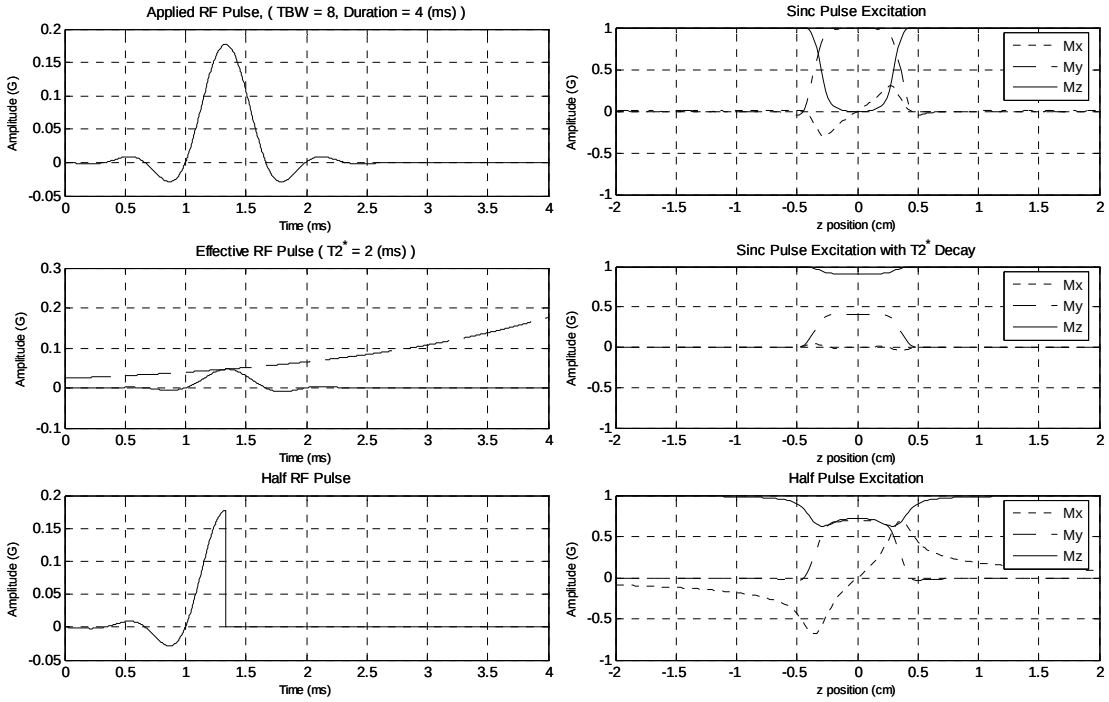

Figure 5 RF pulses & Slice Profiles (TBW=8, Duration=4ms)

3.2 OFF-RESONANCE

Off-resonance of 0Hz (On-resonance), -220Hz, -440Hz -660Hz are used here. Figure 6 and Figure 7 show Mx and My components in Applied and effective pulses are significantly affected by off-resonance. But Figure 8 shows that half-pulse excitation has, although we can observe some Mx component, robust profile.

3.3 FLOWING SPINS

Like off-resonance case, Flow velocity also affects the degree of profile distortion, which directly relates to the severity of flow artifacts. To understand better the effect of a selective excitation on the behavior of a flowing spin system, it is useful to extend the solution to the Bloch equation to include terms of higher order motion.

A conventional excitation with refocusing has large degree of profile distortion, as shown in Figure 9 and Figure 10, because the longer excitation interval results velocity-dependent phase shifts. In contrast, half-pulse excitation shown in Figure 11 yields a robust profile and remains intact even at the higher velocities. Note that the Mx components cancel out and are not observed because off-resonance effects are ignored.

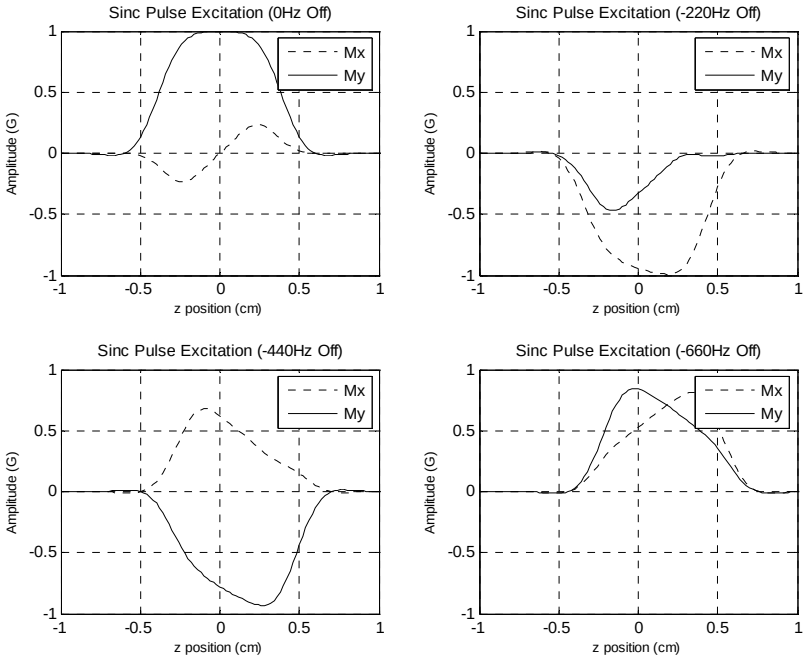

Figure 6 Off-resonance effect for applied sinc pulse excitation (0,-220,-440,-660 Hz off)

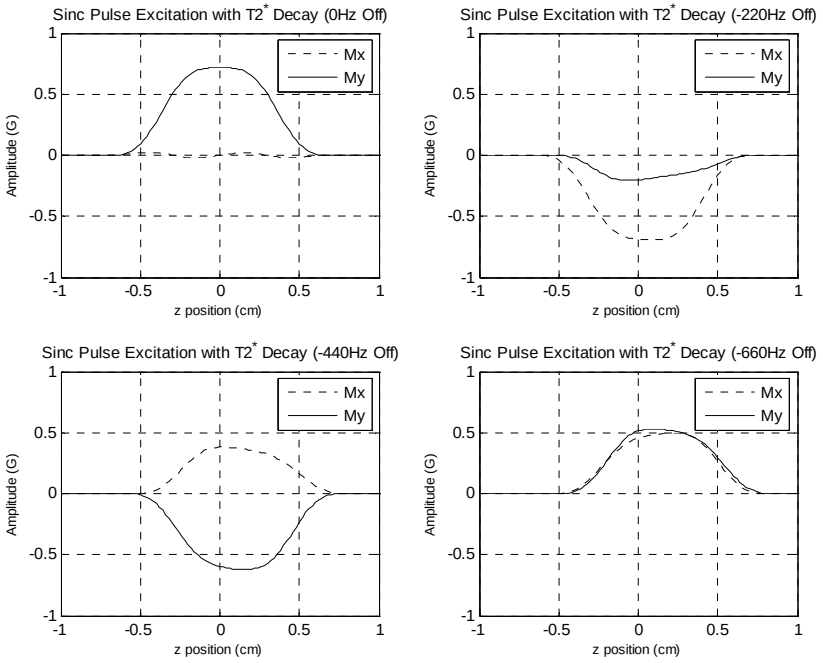

Figure 7 Off-resonance effect for effective sinc pulse excitation (0,-220,-440,-660 Hz off)

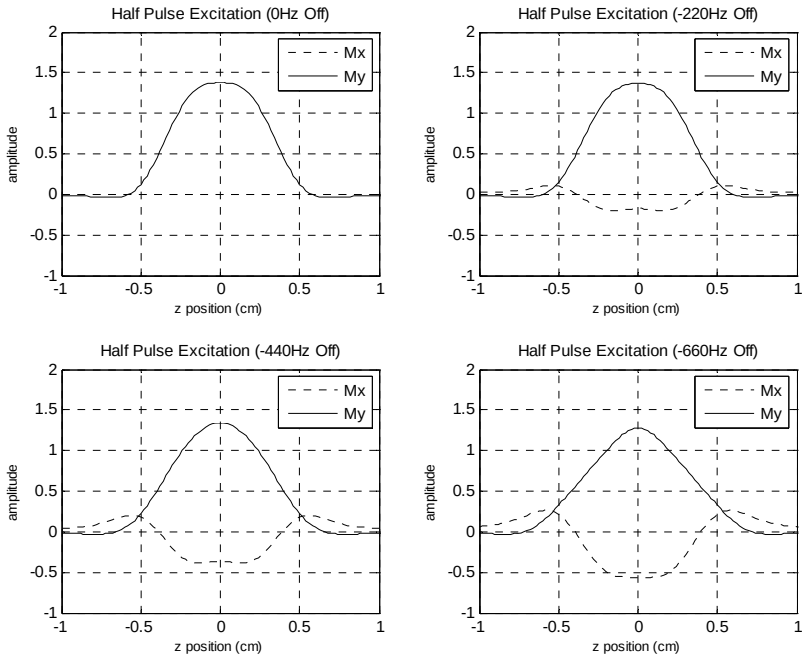

Figure 8 Off-resonance effect for half-pulse excitation (0,-220,-440,-660 Hz off)

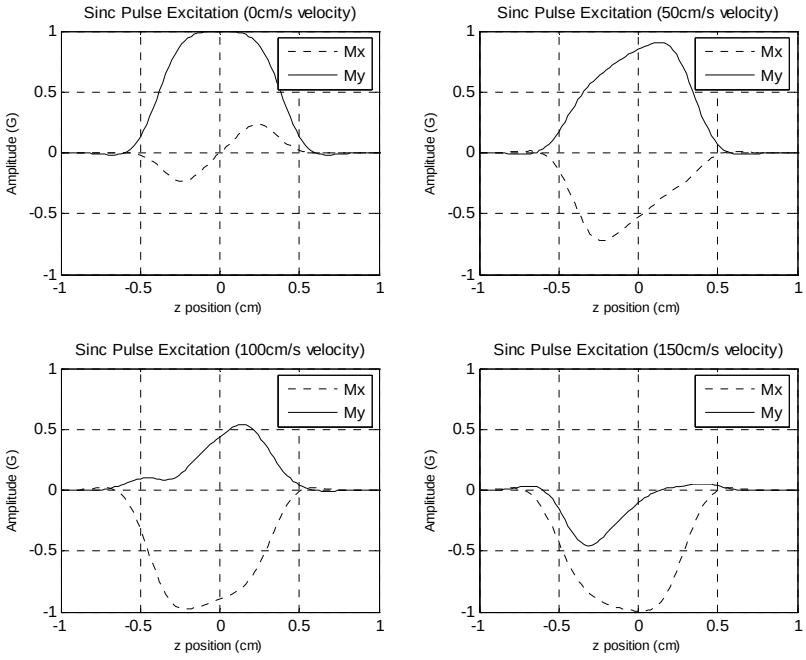

Figure 9 Flowing spins effect for applied sinc pulse excitation (0,50,100,150 cm/s)

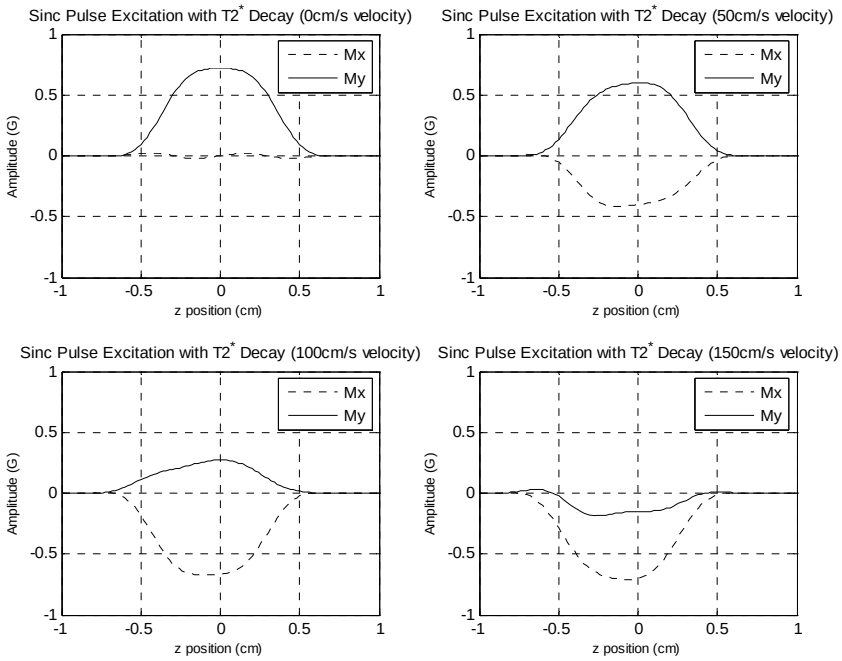

Figure 10 Flowing spins effect for effective sinc pulse excitation (0,50,100,150 cm/s)

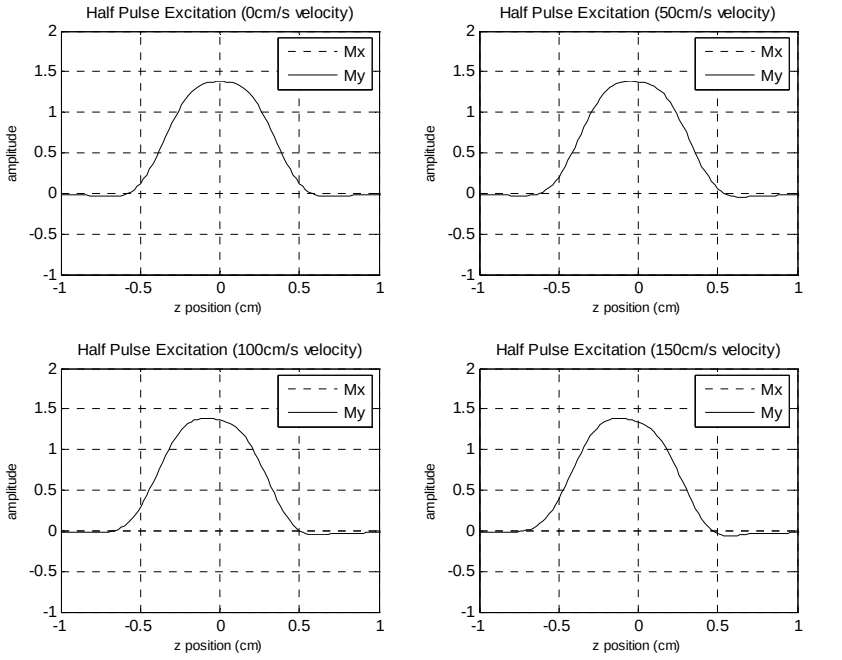

Figure 11 Flowing spins effect for half pulse excitation (0,50,100,150 cm/s)

3.4 LONG T2 SUPPRESSION PULSE

Traditional "T2-weighted contrast" images tend to highlight tissue components with long-T2 values while suppressing those with short-T2 values. Therefore this is better suited towards visualizing components with long-T2 values. In the case of half-pulse, however, we cannot use this technique for T2-wehighted contrast because TE is very short. Currently, three different techniques exist which are capable of solving this problem; Image subtraction, Multi exponential decay analysis, T2-Selective RF Excitation Contrast. Image subtraction, in general, has a poor contrast-to-noise ratio (CNR) performance. Multi-exponential decay analysis tends to have very high signal-to-noise ratio (SNR) demands resulting in excessively long scan times and/or low spatial resolution. [6-9] But T2-Selective RF Excitation Contrast method has no limitation like those.

T2-Selective RF Excitation Contrast was originally proposed by Pauly et al.[10], which adds Long T2 suppression pulse before RF pulse in Figure 2(c) and also adds dephaser before Gz.

First, long low π/2 pulse of length T makes T2 species less than T remain unexcited and the others are completely excited. Excited magnetization then is dephased by dephaser. Therefore remaining magnetization can be imaged with half-pulse sequence.

Using bloch equation, the solution for this pulse can be expressed as follow,

$$m_z(T) = e^{-\frac{\pi}{2}\left(\frac{T}{\pi T_2}\right)}\left[\frac{\frac{T}{\pi T_2}}{\sqrt{\left(\frac{T}{\pi T_2}\right)^2 - 1}}\sinh\left(\frac{\pi}{2}\sqrt{\left(\frac{T}{\pi T_2}\right)^2 - 1}\right) + \cosh\left(\frac{\pi}{2}\sqrt{\left(\frac{T}{\pi T_2}\right)^2 - 1}\right)\right]$$

This is a function of T2/T. If we want to preserve T2 species of 2ms with 80% efficiency, we need 10*2ms=20ms pulse, as shown in Figure 12. We can also approximate the above equation by using below equation. It depends on only RF power.

$$m_z(T) \cong m_0\left(1 - T_2 \int_{-\infty}^{T} (\gamma B_1(t))^2 \, dt\right)$$

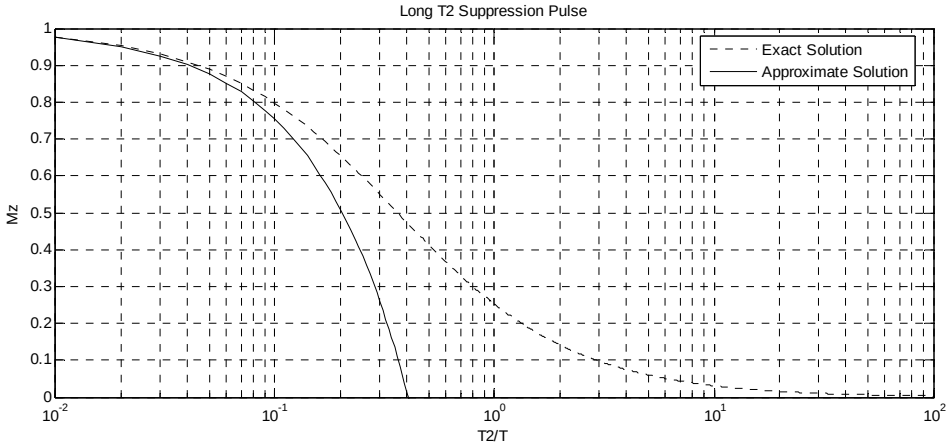

Figure 12 Approximate vs Exact Solution Rectangular Suppression pulse

4. REFERENCE

[1] Nishimura D, Macovski A, Jackson JI, Hu RS, Stevick CA, Axel L.Magnetic resonance angiography by selective inversion recovery using a compact gradient echo sequence. Magn Reson Med 1988;8:96–103.

[2] Schmalbrock P, Yuan C, Chakeres DW, Kohli J, Pelc NJ. Volume MR angiography: methods to achieve very short echo times. Radiology 1990;175:861–865.

[3] Urchuk SN, Plewes DB. Mechanisms of flow-induced signal loss in MR angiography. J Magn Reson Imaging 1992;2:453–462.

[4] Pauly J, Conolly S, Nishimura D, Macovski A. Slice-selective excitation for very short T2 species. In: Proceedings of the SMRM 8th Annual Meeting, Amsterdam, The Netherlands, 1989:28.

[5] Nielsen HTC, Olcott EW, Nishimura DG. Improved 2D time-of-flight angiography using a radial-line k-space acquisition. Magn Reson Med 1997;37:285–291.

[6] A. Mackay, K. Whittall, J. Adler, D. Li, D. Paty, and D. Graeb, In Vivo Visualization of Myelin Water in Brain by Magnetic Resonance. Magnetic Resonance in Medicine 1994;31:673-677.

[7] K. Whittall , A. Mackay, D. Graeb, R. Nugent, D. LI, and D. Paty, In Vivo Measurement of T2 Distributions and Water Contents in Normal Human Brain. Magnetic Resonance in Medicine 1997;37:34-43.

[8] K. Whittall and A. Mackay, Quantitative Interpretation of NMR Relaxation Data. Journal of Magnetic Resonance 1984;134:134-152.

[9] S. Graham, P. Stancheva, and M. Bronskill, Feasibility of Multi component T2 Relaxation Analysis using Data Measured on Clinical MR Scanners. Magnetic Resonance in Medicine, 1996;35:370-378.

[10] J. Pauly, S. Conollya, and A. Macovski, , Suppression of Long-T2 Components for Short-T2 Imaging. Journal of Magnetic Resonance Imaging, 1992;2:145.

[11] H.T. Nielson, G.E. Gold, E.W. Olcott, J.M. Pauly, D.G. Nishimura, Ultra-short echo-time 2D time-of-flight MR angiography using a half-pulse excitation, Magn. Res. Med. 1999;41: 591–599.